

Reconciling cosmic dipolar tensions with a gigaparsec void

Tingqi Cai,^{1,2,*} Qianhang Ding,^{1,2,†} and Yi Wang^{1,2,‡}

¹*Department of Physics, The Hong Kong University of Science and Technology,
Clear Water Bay, Kowloon, Hong Kong, P.R.China*

²*Jockey Club Institute for Advanced Study, The Hong Kong University of Science and Technology,
Clear Water Bay, Kowloon, Hong Kong, P.R.China*

Recent observations indicate a 4.9σ tension between the CMB and quasar dipoles. This tension challenges the cosmological principle. We propose that if we live in a gigaparsec scale void, the CMB and quasar dipolar tension can be reconciled. This is because we are unlikely to live at the center of the void. And a 19% offset from the center will impact the quasars and CMB differently in their dipolar anisotropies. As we consider a large and thick void, our setup can also ease the Hubble tension.

I. INTRODUCTION

The cosmological principle is a fundamental postulate in modern cosmology, assuming that the universe is homogeneous and isotropic on large scales, independent of location of observers [1]. Based on the cosmological principle, the Lambda cold dark matter (Λ CDM) model [2–4] is established and considered as the standard model of cosmology.

With the development of precision cosmology, new observable results show hints of inconsistencies between observations and the cosmological principle, e.g., the detection of cosmic dipole such as cosmic microwave background (CMB) dipole [5] and quasar dipole [6] may be inconsistent and indicate an anisotropic observable universe. Also, the Hubble tension between its local measurements [7, 8] and the value from Planck [9], which may be interpreted as the existence of a local inhomogeneous structure [10, 11]. A fundamental explanation is needed in these problems.

In reconciling the inconsistency between observations and the cosmological principle, a number of models have been proposed, such as introducing new physical scenarios in solving the Hubble tension [12–19] and using the peculiar motion of observers in explaining the cosmic dipole [20, 21]. However, the tension between the CMB dipole and quasar dipole remains unsolved. The amplitude of the quasar dipole is over twice as large as the expected value in kinematic interpretation of the CMB dipole. In same analysis, the inconsistency is reported to be as significant as 4.9σ [6]. Such a large quasar dipole anisotropy still exists after removing the standard kinematic dipole in CMB frame, which may indicate the existence of a local anisotropic structure [22]. Meanwhile, some theoretical attempts have been done in solving this dipolar tension, see [23–25] for details.

The introduction of a Gpc-scale local void changes the story. A local underdense region with us as observers inside could cause additional peculiar motion of nearby supernovae (SNe). A Gpc-scale void makes sure that almost all detected SNe live inside, which biases local measurement of Hubble parameter and ease the Hubble tension (see [10] for more details). Since it is very unlikely for the position of the Milky Way to locate at the exact center of this local void, the observational anisotropy would be induced by an off-center location of observers inside the void [26–28].

In this article, we propose that the amplitude inconsistency between CMB and quasar dipoles can also be explained by our offset from the center of a void. Due to the existence of such an anisotropic spacetime in an off-center void, the detected photons from different directions have experienced different cosmic expansion histories, which causes an anisotropy in their cosmic redshifts. The CMB dipole and quasar dipole, measured from CMB temperature perturbations and hemisphere quasar number counting [29] respectively, could also be in part attributed to the redshift dipole anisotropy. Since the redshift dipole is induced by anisotropic matter distribution inside the void, it reaches a peak value at the boundary of the void. Thus, by considering that we live at an off-center position of a void, the origin of the quasar dipole can be explained, where the void has thick boundary and is as large as the average distance from us to distant quasars. We also provide a first-principle calculation of the intrinsic matter density dipole anisotropy in an off-center local void scenario, which is the origin of the detected cosmic dipole and has a similar behavior to the redshift dipole.

* tcaiac@connect.ust.hk

† qdingab@connect.ust.hk

‡ phyw@ust.hk

II. ORIGIN OF A GPC-SCALE VOID

In standard cosmological scenarios where structures originate from a Gaussian random density field, the presence of a Gpc-scale void is unlikely, due to $\sigma_8 \simeq 0.81$ [30], which shows that the amplitude of fluctuations is statistically suppressed on comoving scales much larger than 10 Mpc. Therefore, a Gpc-scale void, if exists, deserves a distinct primordial origin. Multi-stream inflation [31] is a potential mechanism to produce a Gpc-scale void. Multi-stream inflation can also generate position space features in cosmology, such as multiverse structures [32], CMB cold spot [33], initial primordial black holes clustering [34], and primordial stellar bubbles [35].

In multi-stream inflation, the inflationary trajectory may encounter a barrier, and then bifurcates into two paths, which experience different inflationary potentials. The inflationary dynamics and the void profile is related as follows: (i) The density contrast between in and outside the void is determined by the e-folding number difference between the two trajectories. The trajectory which is now a void has less e-folds of inflation, by $\delta\rho/\rho \sim \delta N$, where δN is the e-folding number difference. (ii) The size of the void is determined by the comoving scale during inflation when bifurcation happened. Thus, the size of the void is a free parameter which can be made Gpc. (iii) The thickness of the boundary between inside and outside the void is determined by the combination scale of the two trajectories. Thus, the void originated from multi-stream inflation can have a smooth profile, which is very important for our model to be consistent with kSZ constraints, as we will emphasize later. An illustration is shown in Fig. 1.

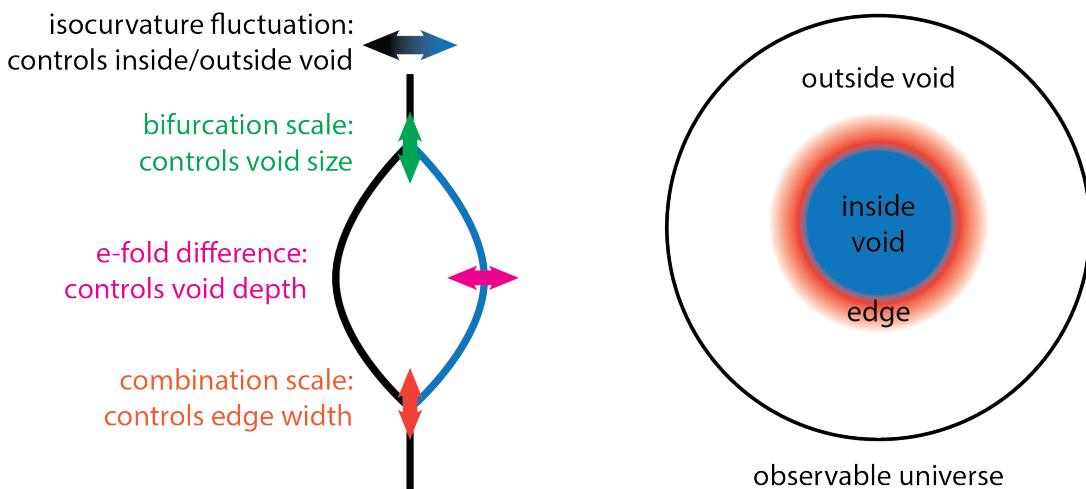


FIG. 1. This figure demonstrates how a cosmic void is generated from multi-stream inflation, which is taken from the Fig. 1 in [10]. *Left panel:* The multi-stream inflation in the primordial universe, where inflationary trajectory encounters a barrier, and bifurcates into two paths with different probabilities. With a larger probability inflaton rolls into the black trajectory, while a smaller probability it rolls into the blue trajectory, which has a larger e-folding number and becomes a void in late universe. *Right panel:* The late-time universe with a void structure embedding arised from the multi-stream inflation.

III. VOID COSMOLOGY

In the universe with a local void embedded, the spacetime is no longer homogeneous and isotropic, therefore, FRW metric cannot be applicable for void cosmology. In order to describe the spacetime in void cosmology, we start from a simple scenario, the shape of void is spherical. In the view of observer at the void center, the spacetime can be described by an inhomogeneous and isotropic metric, which is well-known Lemaitre-Tolman-Bondi (LTB) metric [36–38] as follows,

$$ds^2 = c^2 dt^2 - \frac{R'(r, t)^2}{1 - k(r)} dr^2 - R^2(r, t) d\Omega^2, \quad (1)$$

where $R'(r, t) = \partial R(r, t)/\partial r$. In a homogeneous scenario, spacetime metric can be recovered from LTB metric to FRW metric via $R(r, t) = a(t)r$, $k(r) = kr^2$, where $a(t)$ is the usual scale factor. We follow [39] to apply LTB metric in Einstein equation to obtain the Friedmann equation in these inhomogeneous and isotropic spacetime as follows

$$H(r, t)^2 \equiv \frac{\dot{R}(r, t)^2}{R(r, t)^2} = H_0(r)^2 \left(\Omega_M(r) \frac{R_0(r)^3}{R(r, t)^3} + \Omega_k(r) \frac{R_0(r)^2}{R(r, t)^2} + \Omega_\Lambda(r) \right), \quad (2)$$

where $H_0(r)$ is the space-dependent local Hubble parameter at present cosmic time defined as $H(r, t_0)$ and $R_0(r)$ is defined as $R_0(r) \equiv R(r, t_0)$. $\Omega_X(r) \equiv \rho_X(r)/\rho_c(r)$ with $X = M, k, \Lambda$, representing matter, curvature and dark energy, respectively. The critical energy density is $\rho_c(r) \equiv 3H_0(r)^2/8\pi G$. The density parameters satisfy $\Omega_M(r) + \Omega_k(r) + \Omega_\Lambda(r) = 1$.

In order to describe the void spacetime, the matter density contrast of void is defined as follows

$$\delta \equiv \frac{\rho_M(r) - \rho_M(\infty)}{\rho_M(\infty)}. \quad (3)$$

We follow [16] to parameterize the void profile as

$$\delta(r) = \delta_V \frac{1 - \tanh((r - r_V)/2\Delta_r)}{1 + \tanh(r_V/2\Delta_r)}, \quad (4)$$

where δ_V and r_V are the depth and radius of the void, and Δ_r is the width of the void boundary. Some examples of void profile are shown in Fig. 2,

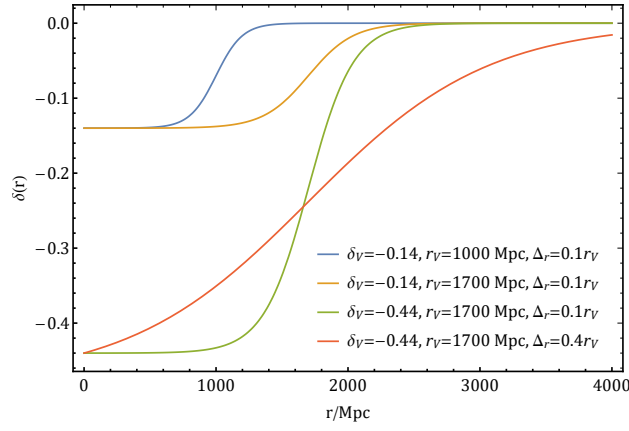


FIG. 2. Some example of void profiles, void depth δ_V determines the matter density contrast, void radius r_V determines the size of low matter density region inside the void, and the width of the void boundary Δ_r determines the thickness of void that transforms from low matter density to high matter density.

We follow [16] to use matter density contrast and current Hubble parameter to express the energy density as

$$\rho_M(r) \propto \Omega_M(r)H_0(r)^2 = \Omega_{M,\text{out}}(1 + \delta(r))H_{0,\text{out}}^2, \quad (5)$$

$$\rho_\Lambda(r) \propto \Omega_\Lambda(r)H_0(r)^2 = (1 - \Omega_{M,\text{out}})H_{0,\text{out}}^2 = \text{const}, \quad (6)$$

$$\rho_k(r) \propto \Omega_k(r)H_0(r)^2 = (1 - \Omega_M(r) - \Omega_\Lambda(r))H_0(r)^2 = H_0(r)^2 - (1 + \Omega_{M,\text{out}})H_{0,\text{out}}^2. \quad (7)$$

Here and hereafter the subscripts “out” denote quantities outside the void. Apply Eqs. (6 – 7) in Eq. (2), it can be expanded as follows,

$$\frac{\dot{R}(r, t)^2}{R(r, t)^2} = \Omega_{M,\text{out}}(1 + \delta(r))H_{0,\text{out}}^2 \frac{R_0(r)^3}{R(r, t)^3} + (H_0(r)^2 - (1 + \Omega_{M,\text{out}})H_{0,\text{out}}^2) \frac{R_0(r)^2}{R(r, t)^2} + (1 - \Omega_{M,\text{out}})H_{0,\text{out}}^2. \quad (8)$$

To fix the gauge, we fix $R(r, t_0) = R_0(r) = r$, which gives

$$\frac{\dot{R}(r, t)^2}{R(r, t)^2} = \Omega_{M,\text{out}}(1 + \delta(r))H_{0,\text{out}}^2 \frac{r^3}{R(r, t)^3} + (H_0(r)^2 - (1 + \Omega_{M,\text{out}})H_{0,\text{out}}^2) \frac{r^2}{R(r, t)^2} + (1 - \Omega_{M,\text{out}})H_{0,\text{out}}^2. \quad (9)$$

Then we integrate Eq. (9), it gives

$$t_B(r) = \int_0^r dR R^{-1} \left[\Omega_M(r)H_0(r)^2 \left(\frac{r}{R}\right)^3 + \Omega_k(r)H_0(r)^2 \left(\frac{r}{R}\right)^2 + \Omega_\Lambda(r)H_0(r)^2 \right]. \quad (10)$$

Here, t_B is the cosmic time since the big bang. Following [16], we set $t_B(r) = t_B = \text{const}$ and $t_0 = t_B$. In the region outside the void $r \gg r_V$, we have $\delta(r) = 0$ and $H_0(r) = H_{0,\text{out}}$, then Eq. (10) can be simplified as follows,

$$t_B = \int_0^1 \frac{da_{\text{out}}}{H_{0,\text{out}} [\Omega_{M,\text{out}} a_{\text{out}}^{-1} + \Omega_{\Lambda,\text{out}} a_{\text{out}}^2]^{1/2}}. \quad (11)$$

Here, a_{out} is the scale factor outside the void. Given a set of $(H_{0,\text{out}}, \Omega_{M,\text{out}}, \Omega_{\Lambda,\text{out}})$, Eq. (11) can determine a fixed t_B , which can be applied in Eq.(10) to obtain $H_0(r)$. Then $R(r, t)$ can be numerically solved from following equation,

$$\frac{\partial R}{\partial t} = R \left[H_0(r)^2 \Omega_M(r) \frac{r^3}{R^3} + H_0(r)^2 \Omega_k(r) \frac{r^2}{R^2} + H_0(r)^2 \Omega_\Lambda(r) \right]^{1/2}. \quad (12)$$

In Eq. (12), we set the initial condition as $R(r, t) = r$ and solve this differential equation backward in time from t_B to $t (< t_B)$ to obtain $R(r, t)$. The dependence of $H(r, t)$ and $R(r, t)$ on redshift can be found by solving null geodesic equation in void spacetime as follows,

$$\frac{dt}{dr} = -\frac{1}{c} \frac{R'(r, t)}{\sqrt{1 - k(r)}}, \quad \frac{1}{1+z} \frac{dz}{dr} = \frac{1}{c} \frac{\dot{R}'(r, t)}{\sqrt{1 - k(r)}}. \quad (13)$$

With the solution of geodesic equation, we can calculate the behavior of cosmological parameters in various void cosmologies and compare them with the parameters in FRW universe, such as Hubble parameter, which can be expressed as $H_{\text{FRW}}(z) = H_{0,\text{out}} \sqrt{\Omega_M(1+z)^3 + \Omega_\Lambda}$. The result is shown in Fig. 3, We can find that different void

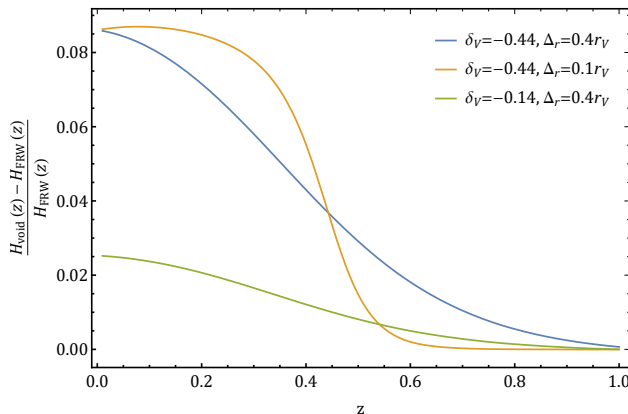


FIG. 3. The difference of Hubble parameter at different redshifts between various void cosmologies and FRW cosmology. δ_V is the depth of the void, Δ_r is the thickness of the void, and the radius of void r_V is set as 1.7 Gpc. The FRW parameter we calculate is $H_0 = 67.4 \text{ km s}^{-1} \text{ Mpc}^{-1}$, $\Omega_M = 0.315$, and $\Omega_\Lambda = 0.685$.

parameters control various behavior of the local universe. A deeper void can effectively increase the value of local Hubble parameter and decrease the Hubble tension. A larger void can affect the local cosmological parameter up to higher redshift, which can help explain the difference of cosmological parameter between local measurements and high redshift measurements. A smoother void can make the behavior of cosmological parameter evolve smoothly, which could help avoid some observational constraints such as constraint from kSZ effect (for more details, see Sec. IV C).

IV. OBSERVATIONAL CONSTRAINTS

The existence of such a Gpc-scale void affects different observations of e.g. Type Ia SNe, baryon acoustic oscillations (BAO) and CMB. The cosmic influence of a void with suitable profile should be consistent with these observational constraints. In following section, we briefly review results in [10] about how observations constrain such a Gpc-scale void (see also [40, 41] and references therein).

A. Type Ia supernovae

Type Ia SNe provide a key measurement for the local universe. From their light curves at redshift $0 < z < 2.3$ [42], the luminosity distance-redshift relation can be determined, which gives a local Hubble parameter $H_0 = 73.3 \pm$

$1.1\text{km s}^{-1}\text{Mpc}^{-1}$ in ΛCDM cosmology [8], while Planck gives Hubble parameter $H_0 = 66.9 \pm 0.6\text{km s}^{-1}\text{Mpc}^{-1}$ [9]. Such a tension in Hubble parameter could be eased by a local Gpc-scale void with the Milky Way inside, which cause nearby SNe to live inside the void and have significant positive peculiar velocities, biasing local measurement of Hubble parameter.

As shown in Fig. 3, the behavior of Hubble parameter inside the local void can help ease Hubble tension. And the profile of the void determines the behavior of Hubble parameter in void spacetime. Especially, when we consider the size of void is up to Gpc scale, nearby Type Ia SNe are located inside this void and their observation result could be explained by such a local void, such as luminosity distance-redshift relation, $D_L(z)$, which is expressed in void cosmology as follows,

$$D_{L,\text{void}}(z) = (1+z)^2 R(r(z), t(z)). \quad (14)$$

Meanwhile, luminosity distance in FRW cosmology is $D_L(z) = (1+z) \int_0^z c/H(z') dz'$. Their local behaviors are shown in Fig. 4. We can find the local behavior of void cosmology with void depth $\delta_V = -0.44$, can well fit local luminosity

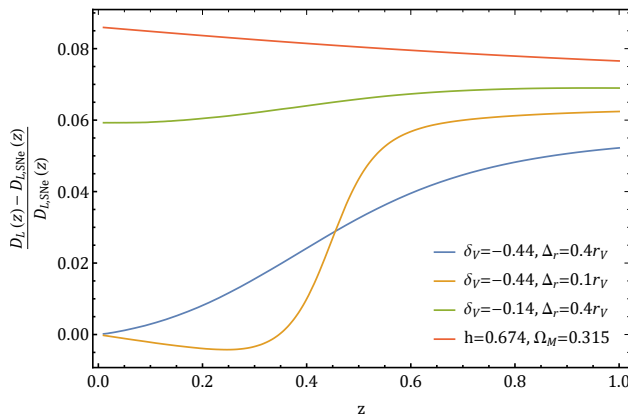


FIG. 4. The difference of luminosity distance-redshift relation between various void cosmologies and FRW cosmology with parameter $(h, \Omega_M, \Omega_\Lambda) = (0.732, 0.3, 0.7)$ from local Type Ia measurement [7], where $h \equiv H_0/100\text{km s}^{-1}\text{Mpc}^{-1}$. δ_V is the depth of the void, Δ_r is the thickness of the void, and the radius of void r_V is set as 1.7Gpc . The FRW cosmology with parameter $(h, \Omega_M, \Omega_\Lambda) = (0.674, 0.315, 0.685)$ from Planck 2018 [30] is also compared.

distance-redshift relation up to $z \sim 0.4$, which shows void cosmology with a large void depth can effectively describe the behavior of the local universe compared with FRW cosmology from Planck 2018 in Fig. 4. Also, the Hubble tension can be solved in such a deeper void with void depth $\delta_V = -0.44$ as shown in Fig. 3, however, some other observations put strong constraints on void depth, see Sec. IV B and IV C for more details.

B. Baryon acoustic oscillations

BAO scale measurements at different redshifts [30, 43–45] provide standard rulers to constrain cosmological models. The observable used from BAO measurement is $(\Delta\theta^2\Delta z)^{1/3}$, which is model independent and can test various cosmologies. In FRW cosmology, it can be expressed as

$$(\Delta\theta^2\Delta z)^{1/3} = \frac{z_{\text{BAO}}^{1/3} r_d}{D_V^{\text{FRW}}(z_{\text{BAO}})}, \quad (15)$$

where r_d is the sound horizon at the drag epoch, and D_V^{FRW} can be expressed in flat FRW case,

$$D_V^{\text{FRW}}(z_{\text{BAO}}) = \frac{1}{H_0} \left[\frac{z_{\text{BAO}}}{E(z_{\text{BAO}})} \left(\int_0^{z_{\text{BAO}}} \frac{dz}{E(z)} \right)^2 \right]^{1/3}, \quad (16)$$

where $E(z) \equiv H(z)/H_0$. Meanwhile, we follow [40] to express $(\Delta\theta^2\Delta z)^{1/3}$ in void cosmology as,

$$(\Delta\theta^2\Delta z)^{1/3} = \left[\frac{(1+z_{\text{BAO}})\dot{R}'_{\text{BAO}}}{R'(r_{\text{BAO}}, t_d(r_{\text{BAO}}))R^2(r_{\text{BAO}}, t_d(r_{\text{BAO}}))} \right]^{1/3} \frac{r_d(r_{\text{BAO}})}{1+z_d(r_{\text{BAO}})}. \quad (17)$$

Here, r_{BAO} , t_{BAO} are radius and time corresponding with z_{BAO} , and R_{BAO} is defined as $R(r_{\text{BAO}}, t_{\text{BAO}})$. $r_d(r)$ and $z_d(r)$ are r -dependent sound horizon and redshift at the drag epoch, respectively.

Based on Eqs. (15) and (17), we can use the observational BAO data to test various FRW and void cosmologies as shown in Fig. 5. We can find that the redshift dependence of spatial curvature in the local void biases a larger

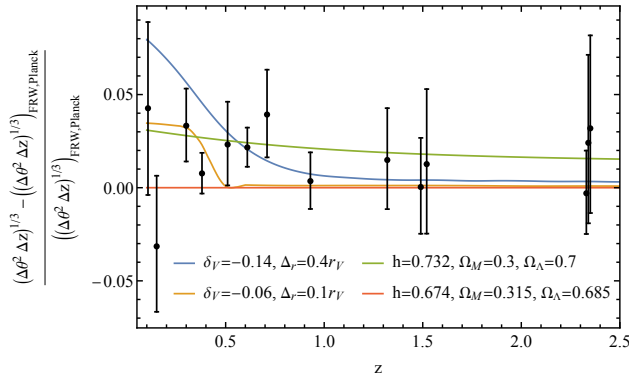


FIG. 5. The difference of $(\Delta\theta^2\Delta z)^{1/3}$ between various void cosmologies and FRW cosmology with parameter $(h, \Omega_M, \Omega_\Lambda) = (0.674, 0.315, 0.685)$ from Planck 2018 [30]. δ_V is the depth of the void, Δ_r is the thickness of the void, and the radius of void r_V is set as 1.7 Gpc. The FRW cosmology with parameter $(h, \Omega_M, \Omega_\Lambda) = (0.732, 0.3, 0.7)$ from local Type Ia measurement [7] is also compared. BAO data for $(\Delta\theta^2\Delta z)^{1/3}$ is taken from various observations [44–50].

value of $(\Delta\theta^2\Delta z)^{1/3}$ and help fit the data better, which is also mentioned in [40]. Also, we can notice that the low matter density at $z < 1$ is favored by BAO data and the void depth is constrained by low redshift measurement of $(\Delta\theta^2\Delta z)^{1/3}$, a void with depth $\delta_V < -0.14$ is disfavored.

C. Kinetic Sunyaev-Zel'dovich effect

A local void could cause the temperature perturbation at small scales of CMB, due to interactions between bulk flow electrons and CMB photons, which is called the kinetic Sunyaev-Zel'dovich (kSZ) effect [51]. The temperature perturbation in direction \hat{n} induced by a local void follows

$$\Delta T_{\text{kSZ}}(\hat{n}) = T_{\text{CMB}} \int_0^{z_e} \delta_e(\hat{n}, z) \frac{V_H(\hat{n}, z) \cdot \hat{n}}{c} \frac{d\tau_e}{dz} dz. \quad (18)$$

Here, $T_{\text{CMB}} = 2.73 \text{ K}$, δ_e is the density contrast of electrons, and τ_e is the optical depth along the line of sight. Follow [52], we set $z_e = 100$ and assume

$$V_H \simeq [\tilde{H}(t(z), r(z)) - \tilde{H}(t(z), r(z_e))] R(t(z), r(z)), \quad (19)$$

where $\tilde{H} = \dot{R}/R'$. The relation between the optical length and redshift can be described as

$$\frac{d\tau_e}{dz} = \sigma_T n_e(z) c \frac{dt}{dz} = \frac{\sigma_T \theta^2 f_b (1 - Y_{\text{He}}/2) \Omega_M [1 + \delta(r(z))]}{24\pi G m_p} c \frac{dt}{dz}. \quad (20)$$

Here, σ_T is the Thomson cross section, f_b is the baryon fraction, Y_{He} is the helium mass fraction, m_p is the proton mass, and θ is defined as $\theta \equiv \tilde{H} + 2H$. Then we can apply Eqs. (19) and (20) in Eq. (18), and use the Limber approximation, to obtain the linear kSZ multipole power C_ℓ as follows,

$$D_\ell = \frac{\ell(\ell+1)}{2\pi} C_\ell \simeq 8\pi \frac{\ell(\ell+1)}{(2\ell+1)^3} \int_0^{z_e} dz \frac{dr}{dz} r(z) \left(\frac{V_H(r)}{c} \frac{d\tau_e}{dz} \frac{dz}{dr} \right)^2 P_\delta \left(\frac{2\ell+1}{2r(z)}, z \right). \quad (21)$$

Here, $P_\delta(k, z)$ is the Λ CDM matter power spectrum, which is calculated from CAMB code [53].

The observed quantity $T_{\text{CMB}}^2 D_\ell$ at $\ell = 3000$ is bounded by $T_{\text{CMB}}^2 D_{3000} = 2.9 \pm 1.3 \mu\text{K}^2$ [54] can be used to put strong constraints on void profiles, which is shown in Fig. 6. It shows a Gpc-scale void can hardly have a significant depth under current observational kSZ limit. However, such a constraint could be eased by increasing the width of the void boundary, this is because the bulk flow electrons in a thick edge void have smaller peculiar velocity than that in a sharp edge void. Therefore, collisions between bulk flow electrons and CMB photons produce weaker temperature distortions in CMB spectrum, which can be found in Eqs. (18) and (19) that a smaller V_H can effectively decrease kSZ temperature distortion and further ease the constraints on void depth.

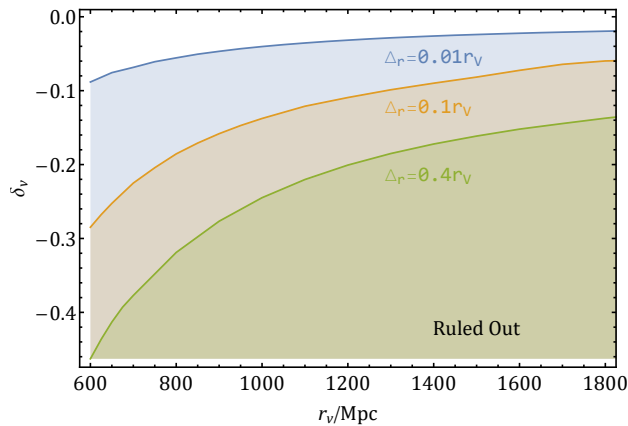


FIG. 6. The kSZ constraints on void profiles, see also [10]. δ_V is the matter density contrast, r_V is void radius and Δ_r is the thickness of the void boundary. The shadow regions are ruled out parameter regions with boundary thicknesses $\Delta_r/r_V = 0.01, 0.1, 0.4$, which is constrained by the requirement $T_{\text{CMB}}^2 D_{3000} < 2.9 \mu K^2$. We observe that voids with thicker boundaries are significantly less constrained by the kSZ effect.

V. COSMIC DIPOLES

As we have introduced above, due to our off-center position inside the void, the observed spacetime is anisotropy and can induce dipole structure in various cosmic structures, such as CMB at high redshift and quasars at low redshifts. However, various spacetime background at different redshifts could induce inconsistent dipole structures in observations, which causes an observational dipolar tension in the framework of FRW cosmology.

In following part, we focus on the CMB dipole and quasar dipole induced by the off-center observation inside a Gpc-scale void, and explain their observational dipolar tension in void cosmology scenario. The void is modeled by the Lemaitre-Tolman-Bondi (LTB) metric as Eq. (1) and its void profile follows Eq. (4) and the parameter of void profile we consider in this work is $r_V = 3800$ Mpc, $\Delta_r = 0.12 r_V$ and $\delta_V = -0.038$, which is allowed under the BAO and kSZ constraints.

A. CMB Dipole

To calculate the dipole signals seen by an off-center observer, it is crucial to specify photon trajectories. We follow [26] to start from the geodesic equation of photons. Due to our off-center position inside the void, the photon trajectories should follow axial symmetry and be independent on the azimuth angle ϕ , then we have following geodesic equations for spacetime coordinate (t, r, θ) ,

$$\frac{d^2 t}{d\lambda^2} + \frac{R' \dot{R}'}{1-k} \left(\frac{dr}{d\lambda} \right)^2 + R \dot{R} \left(\frac{d\theta}{d\lambda} \right)^2 = 0, \quad (22)$$

$$\frac{d^2 r}{d\lambda^2} + \left(\frac{R''}{R'} + \frac{k'}{2-2k} \right) \left(\frac{dr}{d\lambda} \right)^2 + 2 \frac{\dot{R}'}{R'} \frac{dr}{d\lambda} \frac{dt}{d\lambda} - \frac{R(1-k)}{R'} \left(\frac{d\theta}{d\lambda} \right)^2 = 0, \quad (23)$$

$$\frac{d^2 \theta}{d\lambda^2} + 2 \frac{R'}{R} \frac{d\theta}{d\lambda} \frac{dr}{d\lambda} + 2 \frac{\dot{R}}{R} \frac{d\theta}{d\lambda} \frac{dt}{d\lambda} = 0. \quad (24)$$

Here, λ is a parameter defined along the trajectories of photons and k is spacetime curvature. Given the position of the observer and the direction of photon arrival as initial conditions, we can numerically solve the geodesic equations of photons backward in time from the present cosmic time to a past cosmic time. After obtaining the solution of geodesic equation of photons, the cosmic redshift along the trajectory of photon $z(\lambda)$ can be calculated by solving following equation,

$$\frac{dz}{d\lambda} = -(1+z) \frac{d\lambda}{dt} \left[\frac{R' \dot{R}'}{1-k} \left(\frac{dr}{d\lambda} \right)^2 + R \dot{R} \left(\frac{d\theta}{d\lambda} \right)^2 \right]. \quad (25)$$

Then we can calculate the redshift distribution of photons on observational direction \hat{n} from a constant time hypersurface $z(\hat{n}, t)$ [26]. Assuming that the observer is placed in the z -axis with distance d . For a photon hitting the

observer at angle ξ relative to the z -axis, as demonstrated in Fig 7, the corresponding CMB temperature is then directly related to redshift

$$T(\xi) = \frac{T_*}{1 + z(\xi)}, \quad (26)$$

where T_* is the temperature at the last-scattering surface. Then the relative temperature variation is

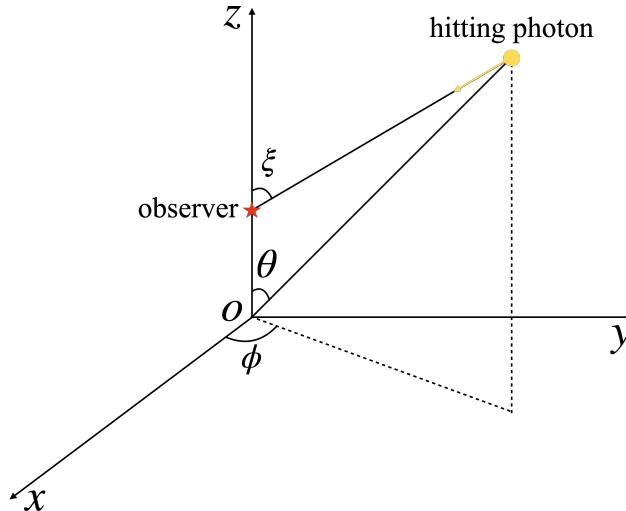


FIG. 7. This figure demonstrates the coordinate system in calculation. The origin of coordinate O is the center of the local void, the red star denotes the observer with distance d to void center, and yellow dot denotes the hitting photon to the observer with an observational angle ξ .

$$\Theta(\xi) \equiv \frac{\Delta T}{\hat{T}} = \frac{T(\xi) - \hat{T}}{\hat{T}}, \quad (27)$$

with the average temperature $\hat{T} = \int d\Omega T(\xi)/4\pi$. Now we can calculate the amplitude of CMB dipole,

$$\mathcal{D} = \frac{2}{\pi} \int_0^\pi \Theta(\xi) \cos \xi d\xi. \quad (28)$$

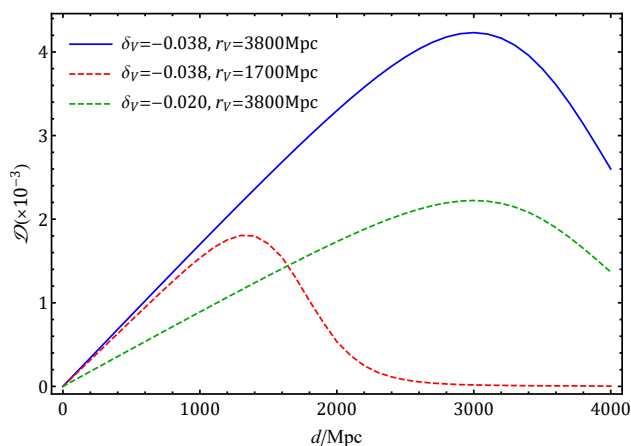


FIG. 8. CMB dipole as a function of observer's location, where d is the distance from the observer to the void center. Different sets of parameters of the void are shown in the labels with the same relative edge width $\Delta_r = 0.12r_V$.

Naturally, the distance from the off-center observer to the center of the void plays an important role. As shown in Fig. 8, the CMB dipole first increases as the observer location becomes further away from the void center, but when

the observer passes the void boundary, the dipole reaches its maximum and starts to decrease, which is conceivable since the observer is no longer inside the void. Meanwhile, the void profile is also significant to the observed CMB dipole. Comparing different curves in Fig. 8, the amplitude of the observed CMB dipole is generally smaller for a shallower void and a larger void radius could produce a larger anisotropic region in the universe. We can give a brief constraint to rule out some void profiles, if the maximal value of induced dipole at z_{CMB} is smaller than observed CMB dipole $\mathcal{D}_{\text{max}} < \mathcal{D}_{\text{CMB}}$,¹ which is shown in the left panel of Fig. 9. Also, we can constrain the void profile based on the location of the observer, that is for a given location of the observer inside the void, which kinds of void profile cannot produce the observed CMB dipole. This requirement can be expressed as $\mathcal{D}(d) < \mathcal{D}_{\text{CMB}}$, the constrained regions are shown in the right panel of Fig. 9.

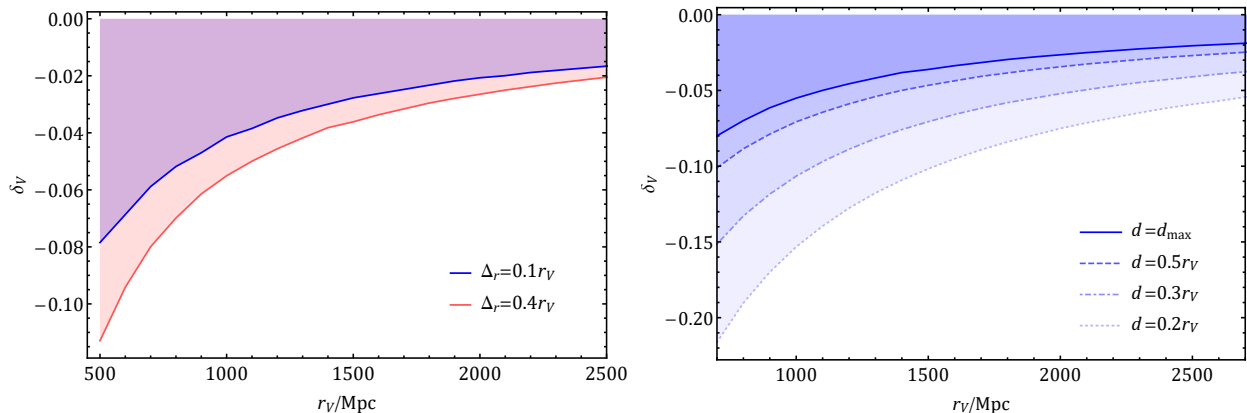


FIG. 9. *Left panel:* Void profile constraints from CMB dipole for different void thickness, where constrained shadow regions satisfy $\mathcal{D}_{\text{max}} < \mathcal{D}_{\text{CMB}}$, and different colors denote the constraints with various void thickness. *Right panel:* Void profile constraints from CMB dipole for different locations of the observer, where constrained shadow regions satisfy $\mathcal{D}(d = d_{\text{abel}}) < \mathcal{D}_{\text{CMB}}$. The types of curve denote the different locations of the observer and d_{max} denotes the location of the observer that can produce the maximal dipole at z_{CMB} . The void thickness is set to $\Delta_r = 0.1 r_V$.

In the left panel of Fig. 9, we can find that, to observe a CMB dipole, a smaller size void requires a deeper void depth, meanwhile a larger size void only needs a shallower depth. This is consistent with our understanding, for two void profiles with same depth and thickness, but different void radius, a larger void radius can produce a larger CMB dipole, as blue solid curve and red dashed curve in Fig. 8. In the right panel of Fig. 9, we can find that, in order to obtain the observed value of CMB dipole, if we are close to the void center, the void depth must be large to achieve the CMB dipole value. It also shows that our distance to the void center strongly depends on the void profile.

As in the previous setting, we consider the parameter of void profile $(r_V, \Delta_r, \delta_V) = (3.8 \text{ Gpc}, 0.46 \text{ Gpc}, -0.038)$. In this benchmark model, the amplitude of detected CMB dipole $\mathcal{D} \simeq 1.23 \times 10^{-3}$ [5] corresponds with the location of the observer is 723 Mpc away from the center of the void, which we will use in following discussion. We need to pay attention to the location of the observer, it is a 19% offset from the void center. Although it is relatively close to the void center, it does not have the coincidence problem, as we have emphasized in the right panel of Fig. 9, the distance to the void center depends on void profile, and this 19% offset is only the value in our benchmark model, a realistic location of the observer needs the future observations on this void profile.

As the LTB metric is isotropic, the orientation of CMB dipole seen by an off-center observer is the same as the direction from the void center to the observer. We can simply set the position direction of the off-center observer to be consistent with CMB dipole, which is $(l, b) = (264^\circ, 48^\circ)$ in galactic coordinate [5]. Fig. 10 shows an example plot of the CMB dipole seen by an observer located 723 Mpc from the center.

Note that this method can be extended from CMB where $z = 1100$ to cosmic dipoles corresponding to lower redshifts, as long as the observable signal is related to redshift in the same way as temperature in Eq.(26), such dipole relation is shown in Fig. 11. We can find that, the amplitude of induced cosmic dipole reaches maximum around $z = 1$, just at the edge of the void. This is because the matter density contrast achieves its maximal value around the void boundary, which strongly increases the spacetime anisotropy and enhances the dipole structure in the redshift distribution of observable signals. When the source gets away from the void, the amplitude of the dipole becomes stable, which corresponds with measured CMB dipole $\mathcal{D} \simeq 1.23 \times 10^{-3}$, since the source can be approximately considered to be at infinity.

¹ In this constraint, we mainly focus on the imprint of local void on CMB dipole, so we ignore the contribution from the peculiar velocity of solar system. Once considering the effect of peculiar velocity, this constraint would be weakened or strengthened, depends on direction of the peculiar motion.

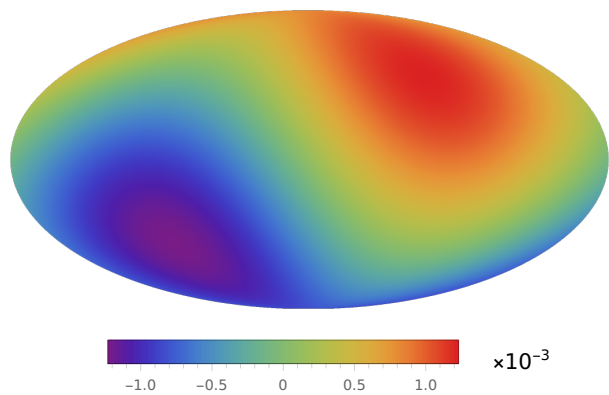


FIG. 10. Observed CMB dipole in the view of an off-center observer. The distance of the observer from void center is set to be 723 Mpc and the position direction from void center to the observer is set to $(264^\circ, 48^\circ)$ in galactic coordinates, which is coincide with measured CMB dipole direction.

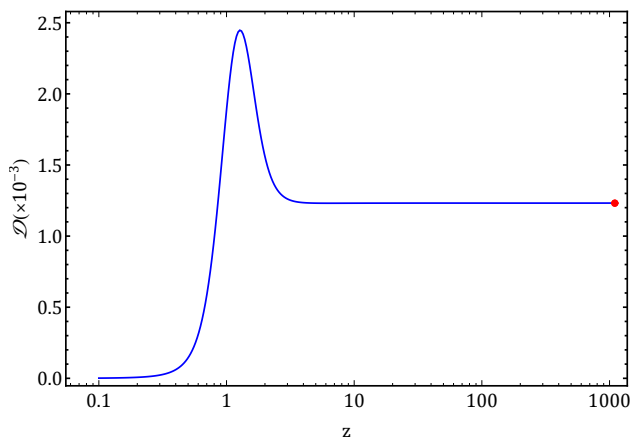


FIG. 11. Induced redshift dipole in the view of an off-center observer. The distance of the observer from void center is set to be 723 Mpc and void profile is $(r_V, \Delta_r, \delta_V) = (3.8 \text{ Gpc}, 0.46 \text{ Gpc}, -0.038)$. The red data point is observed CMB dipole $\mathcal{D} = (1.23 \pm 0.00036) \times 10^{-3}$ at redshift $z = 1100$ [5].

B. Quasar Dipole

Besides CMB, distant sources like quasars can also form dipoles in void cosmology. For CMB, the dipole appears in its temperature anisotropy, while for quasar, the dipole appears in number counting anisotropy. That is to say angular number density $dN/d\Omega$ is different when observer looks into different direction ξ .

Such anisotropy can be derived using similar methods in kinematic interpretation of the quasar dipole [20]. Consider an off-center observer in a local void, the frequency of observed photons ν_o is redshifted from the emission frequency ν_e as

$$\nu_o(\xi) = \frac{\nu_e}{1 + z(\xi)}. \quad (29)$$

As Eq. (27), we can calculate variance of observed frequency of photons as,

$$\Theta \equiv \frac{\Delta\nu_o}{\widehat{\nu}_o} = \frac{\nu_o(\xi) - \widehat{\nu}_o}{\widehat{\nu}_o}, \quad (30)$$

where $\widehat{\nu}_o = \int d\Omega \nu_o(\xi)/4\pi$, then we define mean redshift $\bar{z} \equiv \nu_e/\widehat{\nu}_o$, which transforms Eq. (29) into

$$\nu_o = \widehat{\nu}_o \kappa(\xi), \quad (31)$$

where $\kappa(\xi) = (1 + \bar{z})/(1 + z(\xi))$. Such an angular-dependent frequency shift is induced by the redshift anisotropy in an off-center void. This causes the anisotropy in power-law spectral energy distribution of the source $S \propto \nu^{-\alpha}$ and a

cumulative power-law distribution above a limiting apparent flux density $N(> S) \propto S^{-x}$. The observed solid angle can be approximated to $d\Omega_o \simeq d\Omega_e \kappa(\xi)^{-2}$ [55]. Accordingly, the observed angular number density is

$$\left(\frac{dN}{d\Omega}\right)_o \simeq \left(\frac{dN}{d\Omega}\right)_e \kappa(\xi)^\gamma, \quad (32)$$

where the index $\gamma = 2 + x(1 + \alpha)$. Following [22], we set $\alpha = 1.06$, $x = 1.89$. The averaged angular number density can be integrated

$$\left(\frac{dN}{d\Omega}\right)_a = \frac{1}{4\pi} \int \left(\frac{dN}{d\Omega}\right)_o d\Omega. \quad (33)$$

The relative variation is

$$\Theta(\xi) = \frac{\Delta(dN/d\Omega)}{(dN/d\Omega)_a} = \frac{(dN/d\Omega)_o - (dN/d\Omega)_a}{(dN/d\Omega)_a}, \quad (34)$$

then the amplitude of quasar dipole can be calculated as Eq. (28), which gives a quasar number dipole at redshift $z \simeq 1.2$ around $\mathcal{D} \simeq 1.42 \times 10^{-2}$ for an observation at the location of 732 Mpc away from void center with void profile $(r_V, \Delta_r, \delta_V) = (3.8 \text{ Gpc}, 0.46 \text{ Gpc}, -0.038)$.

Similar to the temperature dipole, this dipole comes from $\kappa(\xi)$ term, due to redshift distribution in difference directions. Just as redshift dipole behavior in Fig. 11, it is clear that there is a peak for the dipole anisotropy around $z = 1$, due to the existence of a Gpc-scale local void. Therefore, when considering kinematic interpretations of quasar dipoles, such a peak dipole anisotropy induced by an off-center void can cause a larger amplitude in the quasar dipole. This reconciles the peculiar velocity inconsistency between the quasar and CMB dipoles.

In principle, there is an intrinsic matter distribution anisotropy in the view of an off-center observer inside the void and it is the origin of the observed quasar dipole. If we assume that the number density of quasars is determined by their surrounding matter density, the amplitude of quasar dipole should be similar to the amplitude of angular matter density dipole. In calculating angular matter density in a local void, the mass term is the matter density times the observed volume elements and the angular term is the observed solid angle, which can be expressed as follows,

$$\frac{dM}{d\Omega}(\xi) = \frac{\rho dS dt}{d\Omega} = \frac{\rho \sqrt{\frac{R'^2}{1-k} dr^2 + R^2 d\theta^2} R \sin \theta d\phi dt}{\sin \xi d\xi d\phi} = \rho \sqrt{\frac{R'^2}{1-k} \left(\frac{dr}{d\xi}\right)^2 + R^2 \left(\frac{d\theta}{d\xi}\right)^2} R \frac{\sin \theta}{\sin \xi} dt, \quad (35)$$

where $dS = \sqrt{R'^2/(1-k)dr^2 + R^2 d\theta^2} R \sin \theta d\phi$ is the area element perpendicular to the trajectory direction of hitting photon, and dt is the physical time interval between two nearby constant time hypersurface. Relative variation and dipole amplitude can be therefore calculated as previously discussed. The results are shown in Fig. 12.

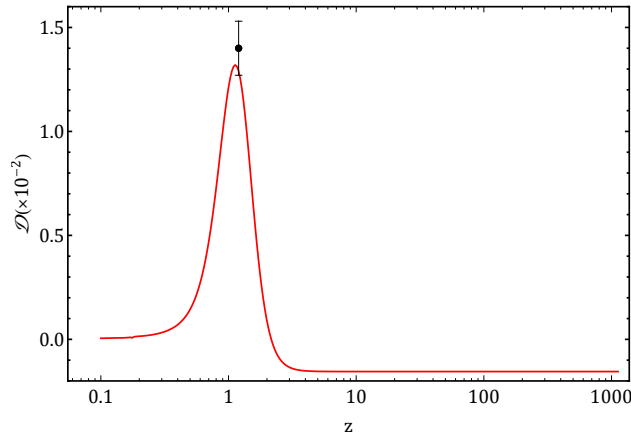


FIG. 12. Angular matter density dipole as a function of redshift. The observer is located at 732 Mpc from the void center and void profile is $(r_V, \Delta_r, \delta_V) = (3.8 \text{ Gpc}, 0.46 \text{ Gpc}, -0.038)$. The black data point is the quasar dipole $\mathcal{D} = (1.40 \pm 0.13) \times 10^{-2}$ at the mean redshift of quasars $z = 1.2$ [22].

In Fig. 12, we can find the angular matter density produces a dipole value $\mathcal{D} \simeq 1.29 \times 10^{-2}$ in the local void scenario, which is consistent with the observed quasar number dipole within 1σ at redshift $z = 1.2$, which is the mean redshift

of observed quasars [56]. However, the angular matter density dipole becomes a negative value when calculating the dipole value outside the local void. Mathematically, this is because the solid angle along the trajectory of hitting photon is smaller than the observational solid angle in the dipolar direction. Physically, due to the curved trajectory of photons, less matter can be observed within a certain solid angle in the direction of dipole, while more matter can be detected in the opposite direction. Also compare with above calculated quasar dipole based on redshift anisotropy dipole, the amplitude of these two dipolar anisotropies takes similar values around $z = 1.2$, it shows the angular matter density dipole could be a decent approximation to the quasar number dipole. However, due to ignoring the curved trajectories of photons, the approach to calculate quasar dipole via redshift anisotropy distribution cannot extend to the region outside the local void, where Eq. (35) needs to be considered.

Based on above discussion, we can find the allowed parameter ranges of the local void profile, whose induced dipole should satisfy the temperature dipole at the redshift of CMB should be around 1.23×10^{-3} and angular matter density dipole at the mean redshift of observed quasars should be in the range of $(1.40 \pm 0.13) \times 10^{-2}$ as follows,

$$\mathcal{D}_T(z_{\text{CMB}}) = 1.23 \times 10^{-3}, \quad \mathcal{D}_A(z_{\text{quasar}}) = (1.40 \pm 0.13) \times 10^{-2}. \quad (36)$$

According to this condition, the allowed parameter regions of void profiles are shown in Fig. 13, where we set the void thickness as $\Delta_r/r_V = 0.1$. We can find that the allowed ranges of void depth is shallowest at $r_V \simeq 3850$ Mpc, which is corresponding with redshift $z \simeq 1.2$. As we have discussed above, the maximal value of induced dipole appears around the boundary of the local void. If this void boundary is corresponding with the mean redshift of observed quasars, the required void depth that matches observed dipoles should be smallest. For a smaller or larger local void, the maximal induced dipole does not appear at the redshift of observed quasars, so they need a larger void depth to explain observed dipoles.

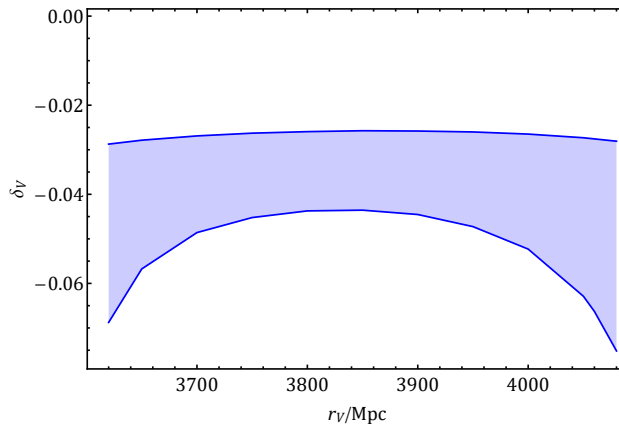


FIG. 13. This figure demonstrates the allowed parameter regions of void profile that can match the observed CMB temperature dipole and quasar number dipole. The void thickness is set as $\Delta_r = 0.1r_V$.

VI. CONCLUSIONS AND REMARKS

To summarize, we propose that the existence of a Gpc-scale local void could affect the validity of the cosmological principle, and reconciling the related dipolar tension. In particular, we study the induced CMB dipole and quasar dipole in the view of an off-center observer inside a Gpc-scale local void. Due to the intrinsic matter distribution anisotropy in an off-center void, the detected photons from different directions have experienced distinct cosmic expansion histories, which causes an anisotropy in their redshift. Such a redshift anisotropy could induce cosmic dipoles by affecting the CMB temperature fluctuation and the analysis in quasar number counting. Also, the intrinsic matter anisotropy in the view of an off-center observer can induce an angular matter density dipole, which should be approximation of quasar number dipole. In our benchmark void model with a 3.8 Gpc void radius, 0.46 Gpc void boundary and -0.038 density contrast, an off-center observer with 723 Mpc away from the void center and relative orientation $(l, b) = (264^\circ, 48^\circ)$ in galactic coordinate, could observe the CMB dipole $\mathcal{D} \simeq 1.23 \times 10^{-3}$ and quasar dipole $\mathcal{D} \simeq 1.29 \times 10^{-2}$. The larger amplitude of quasar dipole than that of CMB dipole is caused by the peak anisotropy at the boundary of the void around $z = 1.2$ and the dipolar tension between them decreases from 4.9σ to 1σ in a Gpc-scale void as shown in Fig. 12.

In this work, motivated by the dipolar tension, we mainly focus on comparing the cosmic dipoles induced by the anisotropy matter distribution in an off-center void. We have not considered the peculiar motion in the local flow, which should affect the CMB and quasar dipoles in the same way and thus does not affect the comparison. Also, we may be moving with respect to the void, which can further extend our model. Finally, if the shape of the void is not spherical, additional anisotropies of higher multipoles may also be introduced.

In our calculation, we use the void profile $(r_V, \Delta_r, \delta_V) = (3.8 \text{ Gpc}, 0.46 \text{ Gpc}, -0.038)$ as a benchmark model, which is consistent with observed CMB dipole and quasar number dipole, when we ignore the peculiar motion of the solar system in the local flow. However, such a void profile cannot fully explain some other observations such as Hubble tension as discussed above. In this case, an overall picture of void profile should take all possible effects into considerations. For instance, as an off-center observer in a local void, we can not only observe the Hubble tension and dipolar tension, but also find the existence of S_8 tension in observation [57, 58]. After considering all possible effects including Hubble tension, dipolar tension (with the contribution from the local flow) and S_8 tension, a physical parameter of this void profile can be determined, which we leave in future study.

It is also important to note that due to the off-center observer in a void, the dipolar anisotropy should consistently exist in many cosmic signals, e.g., Type Ia SNe [27, 59–62], large scale structure [63, 64], 21cm background [65] and gravitational wave background [66, 67]. If we are indeed located in a void, the void profile can be understood better by a combined study of these signals.

ACKNOWLEDGEMENT

We thank Haipeng An and Zhong-Zhi Xianyu for helpful discussion. This work is supported in part by the National Key R&D Program of China (2021YFC2203100), the NSFC Excellent Young Scientist Scheme (Hong Kong and Macau) Grant No. 12022516, and the GRF grant 16303621 by the RGC of Hong Kong SAR.

-
- [1] E. A. Milne, “Kinematics, Dynamics, and the Scale of Time,” *Proc. R. Soc. Lond. Ser. A* **158** no. 894, (Jan., 1937) 324–348.
 - [2] V. C. Rubin and J. Ford, W. Kent, “Rotation of the Andromeda Nebula from a Spectroscopic Survey of Emission Regions,” *Astrophys. J.* **159** (Feb., 1970) 379.
 - [3] M. S. Turner, G. Steigman, and L. M. Krauss, “Flatness of the universe: Reconciling theoretical prejudices with observational data,” *Phys. Rev. Lett.* **52** (Jun, 1984) 2090–2093.
 - [4] C. S. Frenk, S. D. M. White, G. Efstathiou, and M. Davis, “Cold dark matter, the structure of galactic haloes and the origin of the Hubble sequence,” *Nature (London)* **317** no. 6038, (Oct., 1985) 595–597.
 - [5] **Planck** Collaboration, N. Aghanim *et al.*, “Planck 2018 results. I. Overview and the cosmological legacy of Planck,” *Astron. Astrophys.* **641** (2020) A1, [arXiv:1807.06205 \[astro-ph.CO\]](#).
 - [6] N. J. Secrest, S. von Hausegger, M. Rameez, R. Mohayaee, S. Sarkar, and J. Colin, “A Test of the Cosmological Principle with Quasars,” *Astrophys. J. Lett.* **908** no. 2, (2021) L51, [arXiv:2009.14826 \[astro-ph.CO\]](#).
 - [7] A. G. Riess *et al.*, “A 2.4% Determination of the Local Value of the Hubble Constant,” *Astrophys. J.* **826** no. 1, (2016) 56, [arXiv:1604.01424 \[astro-ph.CO\]](#).
 - [8] D. Brout *et al.*, “The Pantheon+ Analysis: Cosmological Constraints,” [arXiv:2202.04077 \[astro-ph.CO\]](#).
 - [9] **Planck** Collaboration, N. Aghanim *et al.*, “Planck intermediate results. XLVI. Reduction of large-scale systematic effects in HFI polarization maps and estimation of the reionization optical depth,” *Astron. Astrophys.* **596** (2016) A107, [arXiv:1605.02985 \[astro-ph.CO\]](#).
 - [10] Q. Ding, T. Nakama, and Y. Wang, “A gigaparsec-scale local void and the Hubble tension,” *Sci. China Phys. Mech. Astron.* **63** no. 9, (2020) 290403, [arXiv:1912.12600 \[astro-ph.CO\]](#).
 - [11] M. Haslbauer, I. Banik, and P. Kroupa, “The KBC void and Hubble tension contradict Λ CDM on a Gpc scale – Milgromian dynamics as a possible solution,” *Mon. Not. Roy. Astron. Soc.* **499** no. 2, (2020) 2845–2883, [arXiv:2009.11292 \[astro-ph.CO\]](#).
 - [12] V. Poulin, T. L. Smith, T. Karwal, and M. Kamionkowski, “Early Dark Energy Can Resolve The Hubble Tension,” *Phys. Rev. Lett.* **122** no. 22, (2019) 221301, [arXiv:1811.04083 \[astro-ph.CO\]](#).
 - [13] J. L. Bernal, L. Verde, and A. G. Riess, “The trouble with H_0 ,” *JCAP* **10** (2016) 019, [arXiv:1607.05617 \[astro-ph.CO\]](#).
 - [14] P. Agrawal, F.-Y. Cyr-Racine, D. Pinner, and L. Randall, “Rock ‘n’ Roll Solutions to the Hubble Tension,” [arXiv:1904.01016 \[astro-ph.CO\]](#).
 - [15] M.-X. Lin, G. Benevento, W. Hu, and M. Raveri, “Acoustic Dark Energy: Potential Conversion of the Hubble Tension,” *Phys. Rev. D* **100** no. 6, (2019) 063542, [arXiv:1905.12618 \[astro-ph.CO\]](#).
 - [16] W. D. Kenworthy, D. Scolnic, and A. Riess, “The Local Perspective on the Hubble Tension: Local Structure Does Not Impact Measurement of the Hubble Constant,” *Astrophys. J.* **875** no. 2, (2019) 145, [arXiv:1901.08681 \[astro-ph.CO\]](#).

- [17] S. Vagnozzi, “New physics in light of the H_0 tension: An alternative view,” *Phys. Rev. D* **102** no. 2, (2020) 023518, [arXiv:1907.07569 \[astro-ph.CO\]](#).
- [18] L. W. Fung, L. Li, T. Liu, H. N. Luu, Y.-C. Qiu, and S. H. H. Tye, “The Hubble Constant in the Axi-Higgs Universe,” [arXiv:2105.01631 \[astro-ph.CO\]](#).
- [19] D. Camarena, V. Marra, Z. Sakr, and C. Clarkson, “A void in the Hubble tension? The end of the line for the Hubble bubble,” *Class. Quant. Grav.* **39** no. 18, (2022) 184001, [arXiv:2205.05422 \[astro-ph.CO\]](#).
- [20] G. F. R. Ellis and J. E. Baldwin, “On the expected anisotropy of radio source counts,” *Mon. Not. Roy. Astron. Soc.* **206** (Jan., 1984) 377–381.
- [21] G. Lavaux, R. B. Tully, R. Mohayaee, and S. Colombi, “Cosmic flow from 2MASS redshift survey: The origin of CMB dipole and implications for Λ CDM cosmology,” *Astrophys. J.* **709** (2010) 483–498, [arXiv:0810.3658 \[astro-ph\]](#).
- [22] N. J. Secrest, S. von Hausegger, M. Rameez, R. Mohayaee, and S. Sarkar, “A Challenge to the Standard Cosmological Model,” *Astrophys. J. Lett.* **937** no. 2, (2022) L31, [arXiv:2206.05624 \[astro-ph.CO\]](#).
- [23] C. Dalang and C. Bonvin, “On the kinematic cosmic dipole tension,” *Mon. Not. Roy. Astron. Soc.* **512** no. 3, (2022) 3895–3905, [arXiv:2111.03616 \[astro-ph.CO\]](#).
- [24] G. Domènech, R. Mohayaee, S. P. Patil, and S. Sarkar, “Galaxy number-count dipole and superhorizon fluctuations,” *JCAP* **10** (2022) 019, [arXiv:2207.01569 \[astro-ph.CO\]](#).
- [25] C. Krishnan, R. Mondol, and M. M. Sheikh-Jabbari, “Dipole Cosmology: The Copernican Paradigm Beyond FLRW,” [arXiv:2209.14918 \[astro-ph.CO\]](#).
- [26] H. Alnes and M. Amarzguioui, “CMB anisotropies seen by an off-center observer in a spherically symmetric inhomogeneous Universe,” *Phys. Rev. D* **74** (2006) 103520, [arXiv:astro-ph/0607334](#).
- [27] H. Alnes and M. Amarzguioui, “The supernova Hubble diagram for off-center observers in a spherically symmetric inhomogeneous Universe,” *Phys. Rev. D* **75** (2007) 023506, [arXiv:astro-ph/0610331](#).
- [28] V. Nistane, G. Cusin, and M. Kunz, “CMB sky for an off-center observer in a local void. Part I. Framework for forecasts,” *JCAP* **12** (2019) 038, [arXiv:1908.05484 \[astro-ph.CO\]](#).
- [29] M. Rameez, R. Mohayaee, S. Sarkar, and J. Colin, “The dipole anisotropy of AllWISE galaxies,” *Mon. Not. Roy. Astron. Soc.* **477** no. 2, (2018) 1772–1781, [arXiv:1712.03444 \[astro-ph.CO\]](#).
- [30] **Planck** Collaboration, N. Aghanim *et al.*, “Planck 2018 results. VI. Cosmological parameters,” *Astron. Astrophys.* **641** (2020) A6, [arXiv:1807.06209 \[astro-ph.CO\]](#). [Erratum: *Astron. Astrophys.* 652, C4 (2021)].
- [31] M. Li and Y. Wang, “Multi-Stream Inflation,” *JCAP* **07** (2009) 033, [arXiv:0903.2123 \[hep-th\]](#).
- [32] S. Li, Y. Liu, and Y.-S. Piao, “Inflation in Web,” *Phys. Rev. D* **80** (2009) 123535, [arXiv:0906.3608 \[hep-th\]](#).
- [33] N. Afshordi, A. Slosar, and Y. Wang, “A Theory of a Spot,” *JCAP* **01** (2011) 019, [arXiv:1006.5021 \[astro-ph.CO\]](#).
- [34] Q. Ding, T. Nakama, J. Silk, and Y. Wang, “Detectability of Gravitational Waves from the Coalescence of Massive Primordial Black Holes with Initial Clustering,” *Phys. Rev. D* **100** no. 10, (2019) 103003, [arXiv:1903.07337 \[astro-ph.CO\]](#).
- [35] Y.-F. Cai, C. Chen, Q. Ding, and Y. Wang, “Ultrahigh-energy gamma rays and gravitational waves from primordial exotic stellar bubbles,” *Eur. Phys. J. C* **82** no. 5, (2022) 464, [arXiv:2105.11481 \[astro-ph.CO\]](#).
- [36] G. Lemaitre, “The expanding universe,” *Annales Soc. Sci. Bruxelles A* **53** (1933) 51–85.
- [37] R. C. Tolman, “Effect of inhomogeneity on cosmological models,” *Proc. Nat. Acad. Sci.* **20** (1934) 169–176.
- [38] H. Bondi, “Spherically symmetrical models in general relativity,” *Mon. Not. Roy. Astron. Soc.* **107** (1947) 410–425.
- [39] J. Garcia-Bellido and T. Haugboelle, “Confronting Lemaitre-Tolman-Bondi models with Observational Cosmology,” *JCAP* **04** (2008) 003, [arXiv:0802.1523 \[astro-ph\]](#).
- [40] T. Biswas, A. Notari, and W. Valkenburg, “Testing the Void against Cosmological data: fitting CMB, BAO, SN and H_0 ,” *JCAP* **11** (2010) 030, [arXiv:1007.3065 \[astro-ph.CO\]](#).
- [41] D. Camarena, V. Marra, Z. Sakr, and C. Clarkson, “The Copernican principle in light of the latest cosmological data,” *Mon. Not. Roy. Astron. Soc.* **509** no. 1, (2021) 1291–1302, [arXiv:2107.02296 \[astro-ph.CO\]](#).
- [42] D. Scolnic *et al.*, “The Pantheon+ Analysis: The Full Dataset and Light-Curve Release,” [arXiv:2112.03863 \[astro-ph.CO\]](#).
- [43] F. Beutler, C. Blake, M. Colless, D. H. Jones, L. Staveley-Smith, L. Campbell, Q. Parker, W. Saunders, and F. Watson, “The 6dF Galaxy Survey: baryon acoustic oscillations and the local Hubble constant,” *Mon. Not. Roy. Astron. Soc.* **416** no. 4, (Oct., 2011) 3017–3032, [arXiv:1106.3366 \[astro-ph.CO\]](#).
- [44] A. J. Ross, L. Samushia, C. Howlett, W. J. Percival, A. Burden, and M. Manera, “The clustering of the SDSS DR7 main Galaxy sample – I. A 4 per cent distance measure at $z = 0.15$,” *Mon. Not. Roy. Astron. Soc.* **449** no. 1, (2015) 835–847, [arXiv:1409.3242 \[astro-ph.CO\]](#).
- [45] **BOSS** Collaboration, S. Alam *et al.*, “The clustering of galaxies in the completed SDSS-III Baryon Oscillation Spectroscopic Survey: cosmological analysis of the DR12 galaxy sample,” *Mon. Not. Roy. Astron. Soc.* **470** no. 3, (2017) 2617–2652, [arXiv:1607.03155 \[astro-ph.CO\]](#).
- [46] F. Beutler, C. Blake, M. Colless, D. H. Jones, L. Staveley-Smith, L. Campbell, Q. Parker, W. Saunders, and F. Watson, “The 6df galaxy survey: baryon acoustic oscillations and the local hubble constant,” *Monthly Notices of the Royal Astronomical Society* **416** no. 4, (2011) 3017–3032.
- [47] M. Blomqvist *et al.*, “Baryon acoustic oscillations from the cross-correlation of $\text{Ly}\alpha$ absorption and quasars in eBOSS DR14,” *Astron. Astrophys.* **629** (2019) A86, [arXiv:1904.03430 \[astro-ph.CO\]](#).
- [48] V. de Sainte Agathe *et al.*, “Baryon acoustic oscillations at $z = 2.34$ from the correlations of $\text{Ly}\alpha$ absorption in eBOSS DR14,” *Astron. Astrophys.* **629** (2019) A85, [arXiv:1904.03400 \[astro-ph.CO\]](#).
- [49] M. Ata *et al.*, “The clustering of the SDSS-IV extended Baryon Oscillation Spectroscopic Survey DR14 quasar sample: first measurement of baryon acoustic oscillations between redshift 0.8 and 2.2,” *Mon. Not. Roy. Astron. Soc.* **473** no. 4,

- (2018) 4773–4794, [arXiv:1705.06373 \[astro-ph.CO\]](#).
- [50] DESI Collaboration, A. G. Adame *et al.*, “DESI 2024 VI: Cosmological Constraints from the Measurements of Baryon Acoustic Oscillations,” [arXiv:2404.03002 \[astro-ph.CO\]](#).
- [51] B. L. Hoscheit and A. J. Barger, “The KBC Void: Consistency with Supernovae Type Ia and the Kinematic SZ Effect in a ALTB Model,” *Astrophys. J.* **854** no. 1, (2018) 46, [arXiv:1801.01890 \[astro-ph.CO\]](#).
- [52] Z.-S. Zhang, T.-J. Zhang, H. Wang, and C. Ma, “Testing the copernican principle with the hubble parameter,” *Physical Review D* **91** no. 6, (2015) 063506.
- [53] A. Lewis, A. Challinor, and A. Lasenby, “Efficient computation of CMB anisotropies in closed FRW models,” *Astrophys. J.* **538** (2000) 473–476, [arXiv:astro-ph/9911177](#).
- [54] E. M. George *et al.*, “A measurement of secondary cosmic microwave background anisotropies from the 2500-square-degree SPT-SZ survey,” *Astrophys. J.* **799** no. 2, (2015) 177, [arXiv:1408.3161 \[astro-ph.CO\]](#).
- [55] D. W. Hogg, “Distance measures in cosmology,” [arXiv:astro-ph/9905116](#).
- [56] F. Marocco, P. R. M. Eisenhardt, J. W. Fowler, J. D. Kirkpatrick, A. M. Meisner, E. F. Schlafly, S. A. Stanford, N. Garcia, D. Caselden, M. C. Cushing, R. M. Cutri, J. K. Faherty, C. R. Gelino, A. H. Gonzalez, T. H. Jarrett, R. Koontz, A. Mainzer, E. J. Marchese, B. Mobasher, D. J. Schlegel, D. Stern, H. I. Teplitz, and E. L. Wright, “The catwise2020 catalog,” *The Astrophysical Journal Supplement Series* **253** no. 1, (Feb, 2021) 8. <https://dx.doi.org/10.3847/1538-4365/abd805>.
- [57] J. Lee, “The effect of primordial antibiasing on the local measurement of the key cosmological parameters,” *Mon. Not. Roy. Astron. Soc.* **440** no. 1, (2014) 119–124, [arXiv:1308.3869 \[astro-ph.CO\]](#).
- [58] K. Ichiki, C.-M. Yoo, and M. Oguri, “Relationship between the CMB, Sunyaev-Zel’dovich cluster counts, and local Hubble parameter measurements in a simple void model,” *Phys. Rev. D* **93** no. 2, (2016) 023529, [arXiv:1509.04342 \[astro-ph.CO\]](#).
- [59] Z. Q. Sun and F. Y. Wang, “Testing the anisotropy of cosmic acceleration from Pantheon supernovae sample,” *Mon. Not. Roy. Astron. Soc.* **478** no. 4, (2018) 5153–5158, [arXiv:1805.09195 \[astro-ph.CO\]](#).
- [60] R. Mohayaee, M. Rameez, and S. Sarkar, “The impact of peculiar velocities on supernova cosmology,” [arXiv:2003.10420 \[astro-ph.CO\]](#).
- [61] C. Krishnan, R. Mohayaee, E. O. Colgáin, M. M. Sheikh-Jabbari, and L. Yin, “Hints of FLRW breakdown from supernovae,” *Phys. Rev. D* **105** no. 6, (2022) 063514, [arXiv:2106.02532 \[astro-ph.CO\]](#).
- [62] P. K. Aluri *et al.*, “Is the Observable Universe Consistent with the Cosmological Principle?,” [arXiv:2207.05765 \[astro-ph.CO\]](#).
- [63] N. Globus, T. Piran, Y. Hoffman, E. Carlesi, and D. Pomarède, “Cosmic-Ray Anisotropy from Large Scale Structure and the effect of magnetic horizons,” *Mon. Not. Roy. Astron. Soc.* **484** no. 3, (2019) 4167–4173, [arXiv:1808.02048 \[astro-ph.HE\]](#).
- [64] K. Migkas, F. Pacaud, G. Schellenberger, J. Erler, N. T. Nguyen-Dang, T. H. Reiprich, M. E. Ramos-Ceja, and L. Lovisari, “Cosmological implications of the anisotropy of ten galaxy cluster scaling relations,” *Astron. Astrophys.* **649** (2021) A151, [arXiv:2103.13904 \[astro-ph.CO\]](#).
- [65] A. Cooray, “21-cm Background Anisotropies Can Discern Primordial Non-Gaussianity,” *Phys. Rev. Lett.* **97** (2006) 261301, [arXiv:astro-ph/0610257](#).
- [66] NANOGrav Collaboration, Z. Arzoumanian *et al.*, “The NANOGrav 12.5 yr Data Set: Search for an Isotropic Stochastic Gravitational-wave Background,” *Astrophys. J. Lett.* **905** no. 2, (2020) L34, [arXiv:2009.04496 \[astro-ph.HE\]](#).
- [67] NANOGrav Collaboration, G. Agazie *et al.*, “The NANOGrav 15 yr Data Set: Evidence for a Gravitational-wave Background,” *Astrophys. J. Lett.* **951** no. 1, (2023) L8, [arXiv:2306.16213 \[astro-ph.HE\]](#).